To Appear in AJ
Preprint typeset using LaTeX style emulateapj v. 04/17/13

arXiv:1605.06517v1 [astro-ph.SR] 20 May 2016

AN AO-ASSISTED VARIABILITY STUDY OF FOUR GLOBULAR CLUSTERS †

R. Salinas[1,2], R. Contreras Ramos[3,4], J. Strader[2],
P. Hakala[5], M. Catelan[3,4], M. B. Peacock[2] and M. Simunovic[4]
[1] Gemini Observatory, Casilla 603, La Serena, Chile
[2] Department of Physics and Astronomy, Michigan State University, East Lansing, MI 48824, USA
[3] Millennium Institute of Astrophysics, Av. Vicuña Mackenna 4860, 782-0436 Macul, Santiago, Chile
[4] Instituto de Astrofísica, Pontificia Universidad Católica de Chile, Av. Vicuña Mackenna 4860, 782-0436 Macul, Chile and
[5] Finnish Centre for Astronomy with ESO, University of Turku, Väisäläntie 20, FI-21500 PIIKKIÖ, Finland
Draft version May 24, 2016

ABSTRACT

The image subtraction technique applied to study variable stars in globular clusters represented a leap in the number of new detections, with the drawback that many of these new light curves could not be transformed to magnitudes due to the severe crowding. In this paper we present observations of four Galactic globular clusters, M 2 (NGC 7089), M 10 (NGC 6254), M 80 (NGC 6093) and NGC 1261, taken with the ground-layer adaptive optics module at the SOAR Telescope, SAM. We show that the higher image quality provided by SAM allows the calibration of the light curves of the great majority of the variables near the cores of these clusters as well as the detection of new variables even in clusters where image-subtraction searches were already conducted. We report the discovery of 15 new variables in M 2 (12 RR Lyrae stars and 3 SX Phe stars), 12 new variables in M 10 (11 SX Phe and one long-period variable) and one new W UMa-type variable in NGC 1261. No new detections are found in M 80, but previous uncertain detections are confirmed and the corresponding light curves are calibrated into magnitudes. Additionally, based on the number of detected variables and new *HST*/UVIS photometry, we revisit a previous suggestion that M 80 may be the globular cluster with the richest population of blue stragglers in our Galaxy.

Keywords: globular clusters: individual (M 2 = NGC 7089), globular clusters: individual (M 10 = NGC 6254), globular clusters: individual (M 80 = NGC 6093), globular clusters: individual (NGC 1261), stars: variables: delta Scuti, stars: variables: RR Lyrae

1. INTRODUCTION

The study of variable stars in crowded environments (e.g. globular clusters) has a long discovery history that was boosted by the introduction of image subtraction techniques (e.g. Tomaney & Crotts 1996; Alard & Lupton 1998; Alard 2000) that allow the discovery of variable stars even in the cores of dense clusters. The standard approach in this technique is to convolve a good seeing image, after image registration, to match its point spread function (psf) to a series of poorer seeing images, before the image subtraction which leads to images where, in principle, only the sources that change within the time scale of the observations, such as transients or variable stars, are left.

Even though image subtraction has an impressive ability for the *detection* of new variables in crowded environments (e.g. Contreras et al. 2005), for many of these stars, crowding and blending make it extremely difficult, if not outright impossible, to transform the relative flux light curves provided by image subtraction into magnitudes (e.g. Baldacci et al. 2005; Corwin et al. 2006; Lázaro et al. 2006), often leaving out of reach much of the information that could be obtained from them (e.g. amplitudes, mean magnitudes, color-magnitude diagram positions, and even information on cluster membership).

In this paper we explore the use of time–series photometry aided by adaptive optics (AO) to obtain sharper images in four Galactic globular clusters: M 2 (NGC 7089), M 10 (NGC 6254), M 80 (NGC 6093) and NGC 1261. Sharper images allow to obtain absolute photometry of a larger number of stars in crowded environments and therefore a calibration of the light curves into standard magnitudes.

We present the instruments used and the data obtained together with its reduction in Section 2, while the detection of variables is presented in Section 3. Periods and classification for the new variables are given in Section 4. Section 5 presents a re-assessment of the blue straggler (BS) content of the dense cluster M 80, while a summary is given in Section 6.

2. OBSERVATIONS AND DATA REDUCTION

2.1. *SOAR/SAM: AO optical imaging*

Time series imaging of M 2, M 10, M 80 and NGC 1261 were obtained using the SOAR Adaptive Module (SAM) coupled with its Imager (SAMI), installed at the SOAR 4.1m telescope at Cerro Pachón, Chile. SAM is a ground layer adaptive optics system correcting atmospheric turbulence near the ground. Technical details of the instrument can be seen in Tokovinin et al. (2010, 2012). SAMI provides a field-of-view (FOV) of $3' \times 3'$ with a pixel scale of $0.0455''$. Observations of M 2, M 10 and M 80 were taken with a 2×2 binning, while the NGC

rsalinas@gemini.edu

†Based on observations obtained at the Southern Astrophysical Research (SOAR) telescope, which is a joint project of the Ministério da Ciência, Tecnologia, e Inovação (MCTI) da República Federativa do Brasil, the U.S. National Optical Astronomy Observatory (NOAO), the University of North Carolina at Chapel Hill (UNC), and Michigan State University (MSU).

Table 1
Observing log

Cluster	N×Exptime g (seconds)	r (seconds)	i (seconds)	UT date (mm.dd.yyyy)	Time span (hours)
M 2	24 × 30	3 × 30	228 × 30	07.21.2015	2.84
M 10	20 × 60	2 × 60	278 × 60	07.21.2015	6.65
M 80	3 × 60	300 × 60 + 15×80	3 × 60	04.23.2014	5.98
NGC 1261	13 × 90	87 × 60	–	12.07.2014	2.36

1261 images were unbinned.

Table 1 gives an observing log indicating dates, filters, exposure times and the total time span of observations. Time series imaging was conducted primarily using the SDSS r and i filters, selected as a compromise between the improvement in the image quality given by SAM (better to redder wavelengths), the desire to study, among others, pulsating *blue* stragglers and the sky brightness during gray time. Additional SDSS g images were taken to place the variables on color-magnitude diagrams and gain further insight into their nature (Section 4).

The time span of the observations varied from cluster to cluster, being at most six hours. This is inadequate for a good description of the complete light curve of RR Lyrae (RRL) stars ($P \sim 13$ hours for ab pulsators and ~ 7 hours for c pulsators) commonly found in metal-poor clusters, but sufficient for their detection and, albeit uncertain, classification. For short-period variables like SX Phoenicis-type stars (hereafter SX Phe), this time span covers about 2–6 complete pulsation cycles, sampling the complete light curve and allowing good period determination. This dataset is inadequate for long–period variables such as Miras or the brighter type II Cepheids, including W Vir and RV Tau stars (e.g. Catelan & Smith 2015).

The image quality that can be achieved with SAM is exemplified in Fig. 1 for the cluster M 80. The lower panel shows the variation of the natural seeing (black rhombi) and the average FWHM as measured using the GEMSEEING task within IRAF for each image (green squares for r images, red for i and blue for g), during the time span of the M 80 observations. Even though at the beginning of the observations the improvement was only of the order of 0.1″, once the natural conditions dropped to around 0.6″ seeing, SAM provided 0.35″ seeing images in the r filter. During the rest of the night, the correction was of the order of 50%. The top panel shows a histogram of the measured FWHM in the r filter. The median FWHM was 0.49″.

Atmospheric conditions were significantly poorer during the other dates. The median measured FWHM for M 2, M 10 and NGC 1261 in (g, r/i), were (0.84″,0.65″), (0.89″,0.69″), and (0.75″,0.68″), respectively.

The Landolt (1992) standard field Mark-A was observed twice (in open loop) in *gri* to obtain a calibration into the standard system during the M 80 run. Magnitudes for these stars in the SDSS sytem were provided by Elizabeth Wehner[1]. Given the relatively small FOV of SAMI compared to the Landolt fields, only two Landolt stars were included and the calibration must be considered as approximate. The derived transformation equations, obtained with IRAF/PHOTCAL, were:

$$g_{\rm instr} = g_{\rm std} - 1.063 - 0.065(g_{\rm std} - r_{\rm std})$$
$$r_{\rm instr} = r_{\rm std} - 0.922 - 0.027(g_{\rm std} - r_{\rm std})$$
$$i_{\rm instr} = i_{\rm std} - 0.767 - 0.057(r_{\rm std} - i_{\rm std}),$$

where the rms of each fit is 0.04, 0.07, 0.04 mags respectively.

SOAR/SAMI data were reduced with the Python-based SAMI pipeline, developed by Luciano Fraga at SOAR. The pipeline bias subtracts, flat fields, mosaics the data read by the four SAMI amplifiers and provides a rough astrometric solution. The astrometry was then refined using MSCTPEAK/CCMAP in IRAF.

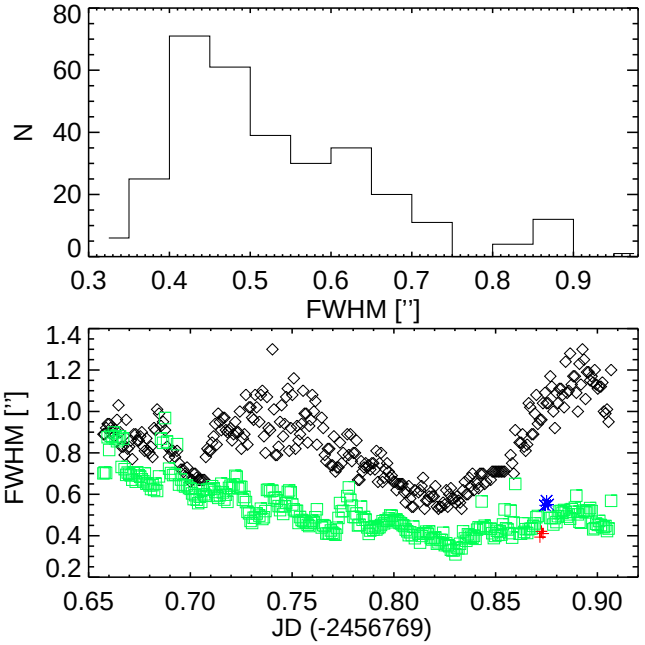

Figure 1. SAM image quality. Top panel: A histogram of the measured FWHM on the complete SAM dataset of M 80. Lower panel: The evolution of seeing as a function of time during the night. Black rhombi are the DIMM seeing measurements while green squares are the measured FWHM on the r SAMI images. Red crosses represent the measurements on the i images, while blue asterisks are the g measurements.

2.2. *HST/UVIS imaging*

M 80 is one of the densest clusters in our Galaxy, with the claim that it hosts the largest amount of blue stragglers of any cluster (Ferraro et al. 1999). As such, a large number of (eclipsing) binaries and pulsating blue stragglers should likely be expected.

[1] http://physwww.mcmaster.ca/~harris/sloan_standards.dat

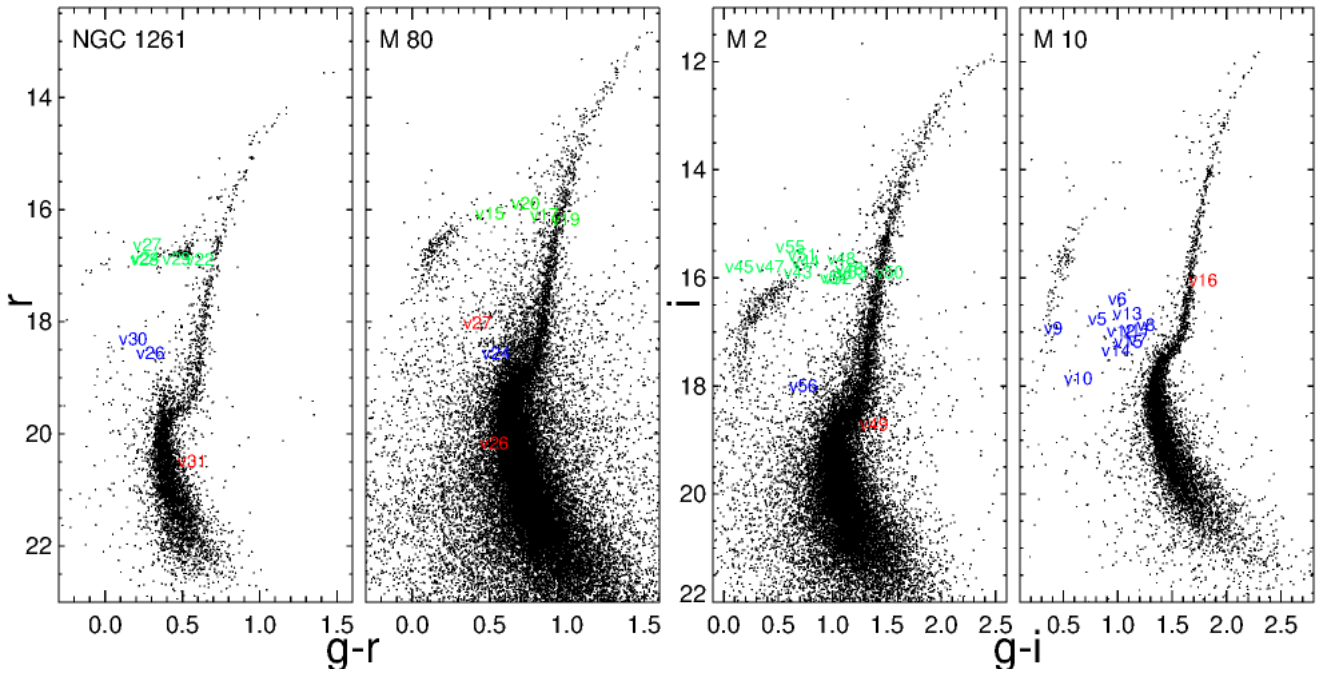

Figure 2. CMDs obtained with ALLFRAME photometry for M 2, M 10, M 80 and NGC 1261 using SAM data. RRL stars are indicated in green, blue stragglers, in blue, while other variables (long period, eclipsing), in red.

Given the high central density of M 80, as an aid to the SAM imaging we also retrieved WFC3/UVIS data from the *HST* public archive that was collected in June 2012 (GO-12605, PI: Piotto) and consist of 10 F255W (855 s), 5 F336W (657 s) and 5 F438W (85 s) exposures. The imaging strategy was optimized to minimize the well-known charge transfer efficiency problems of UVIS (see Piotto et al. 2015, for details).

Stellar photometry of the dark and bias subtracted and flat-fielded data was performed using the online public program IMG2XYM_WFC3UV, which is based on the photometry package developed for the ACS/WFC camera (Anderson & King 2006). This software was specifically designed to perform reduction analysis of the undersampled WFC3 data using empirical psfs. Fluxes and positions were corrected for geometric distortions using the solution given by Bellini et al. (2011). In order to place our catalogue in a common coordinate system we have used astrometric standard stars selected from the third US Naval Observatory CCD Astrograph Catalog (UCAC3, Zacharias et al. 2010) and used CATAXCORR, a program developed at the Bologna Observatory (P. Montegriffo, private communication), to perform roto-translation procedures. Our final catalog consists of highly internally precise photometry and astrometric positions of ∼40000 stars around the center of M80, from the tip of the RGB to ∼4 magnitudes below the main sequence turn off (see Section 5).

3. VARIABLE STARS DETECTION AND PHOTOMETRY

3.1. *Image subtraction*

Variable stars were initially searched using ISIS (v 2.1, Alard 2000), an implementation of the image subtraction technique which registers and matches the point spread function of images before subtraction, over the SAM dataset. A reference frame that is convolved to match the psf of each image was constructed using a handful of images with the lowest FWHM.

Once the convolved reference frame is subtracted from each individual image, ISIS produces a stack of all the absolute residual images where variables can now be searched. We find that a visual inspection of the stacked residuals produces the best results instead of applying a detection threshold on this image (Salinas et al. 2005, 2007), discarding false residuals produced by cosmic rays, bad pixels and saturated stars.

As a further search for variables in the region of the blue stragglers, we searched for variability in the positions of all the blue stragglers as determined from the CMDs using SAMI data (see Fig. 2) as well as the *HST*/UVIS CMD for M 80 (see Section 5). Furthermore, BSs were also identified in the DAOPHOT catalogues from UVIS observations of M 2 and M 10 retrieved from the Hubble Legacy Archive[2]. For NGC 1261 we used the *HST* photometry from Simunovic et al. (2014). The success of this approach is exemplified in NGC 2808, where Catelan et al. (2006) found a higher number of pulsating blue stragglers than other studies which used the same (Corwin et al. 2004) or augmented (Kunder et al. 2013) datasets, but different variable identification approaches.

Relative flux light curves provided by ISIS were then turned into magnitudes using the ALLFRAME photometry (see Section 3.2), following the procedure outlined in Catelan et al. (2013). Calibration of the light curves into the standard system formally requires color information for each epoch. Color variations within a pulsation cycle, for example, for RRL stars, will not be larger than about $V - R = 0.3$ mag (e.g. Kunder et al. 2010). In practice assuming a constant $g-r$ (or $g-i$) color during the calibration introduces a systematic error of ≤ 0.02 mag in r, a value that is smaller than the uncertainty introduced by the calibration equations (Sect. 2.

[2] hla.stsci.edu

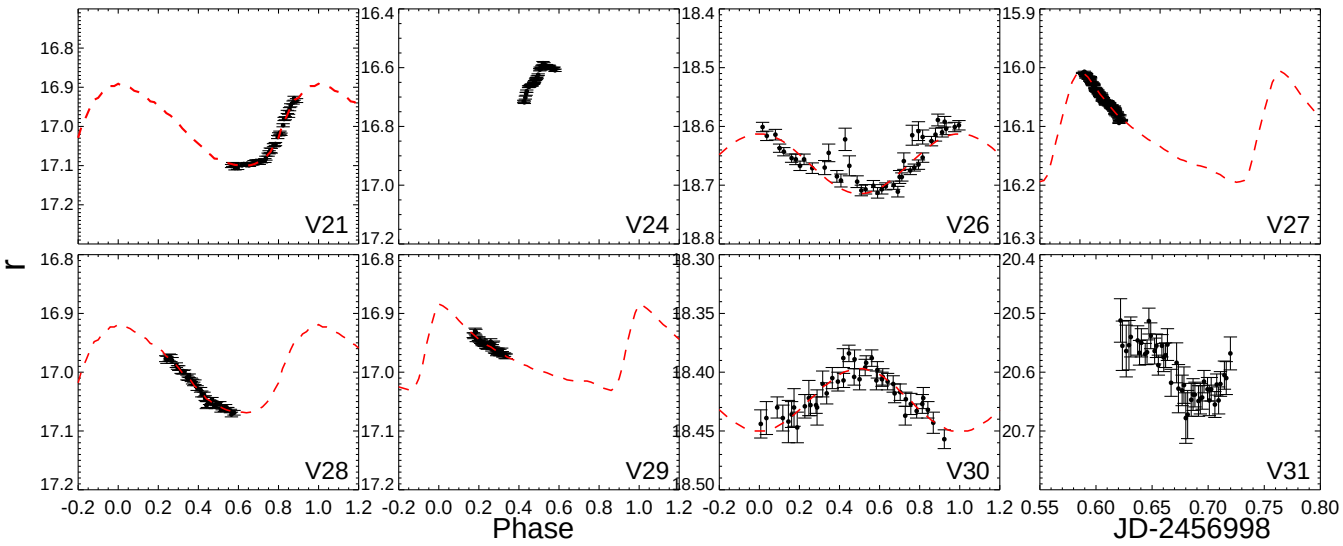

Figure 3. Variables in NGC 1261. V21-V30 were discovered by Salinas et al. (2007), while V31 is a new discovery. Dashed lines indicate the best-fit template. The V31 light curve is not shown phased, but only with its Julian date, given the large uncertainty in its period.

3.2. *PSF photometry*

In order to construct color-magnitude diagrams that help pin down the nature of the found variables and provide the reference magnitudes used to transform the ISIS relative flux light curves into magnitudes, stellar photometry was also conducted using the stand-alone DAOPHOT/ALLSTAR profile-fitting photometry package (Stetson 1987). The psf was constructed by choosing between 50 and 100 bright and isolated stars, which were modeled as a quadratically varying Moffat function (with $\beta = 2.5$) following previous work with SAM (Fraga et al. 2013). The same psf stars were used in all frames for each cluster and their coordinates were transformed using DAOMATCH/DAOMASTER (Stetson 1993) and STILTS (Taylor 2006).

Model psfs and ALLSTAR photometry were then used to obtain improved photometry with ALLFRAME (Stetson 1994), following the procedure described in Salinas et al. (2012). Resulting color-magnitude diagrams for the four clusters can be seen in Fig. 2.

4. KNOWN AND NEWLY FOUND VARIABLES

In this section we give details about the new variable stars detected following the procedure presented in Section 3, as well as quantities not given before for the previously known variables.

Periods for the new variables were determined using the phase dispersion minimization method (Stellingwerf 1978) as implemented in IRAF. No attempt was made to refine the periods for the known variables given the short time span of the observations. Some SX Phe variables are known to pulsate in more than one mode, generating amplitude variations (Eggen 1952; Walraven 1953). Multiple periods in our SX Phe candidates were searched using the standard Lomb-Scargle technique (Scargle 1982).

The limited phase coverage for RRL stars also precludes giving reliable amplitudes and mean magnitudes directly from the data. These quantities were estimated instead, when periods were known, by using the template fitting code of Layden (1998). The code fits ten templates of RRL stars and eclipsing binaries for a given period, giving a χ^2 value that is used to determine the best template, and optionally, its classification. Being the longest period variables, RRab are the most affected by the limited phase coverage and their amplitudes are in many cases underestimated. Even though the templates were set up using observations in V (Layden 1998), the general shape of RRL remains mostly unaltered with passband, changing only their amplitudes, which is taken into acount in the fitting process.

4.1. *NGC 1261*

The variable star content of NGC 1261 was studied by Wehlau & Demers (1977) and Wehlau et al. (1977), finding 18 RRL and one long period variable. A modern image-subtraction search was conducted by Salinas et al. (2007) who further found 4 RRL, 3 SX Phe variables and one more long-period variable. Salinas et al. (2007) provided only relative-flux light curves and periods, so here we give light curves in magnitudes, using the limited phase coverage of our SAMI data, their position on a CMD, and the estimated intensity-weighted mean magnitudes and amplitudes resulting from the template fitting procedure in the case of the RRL. No satisfactory was found for V24. For the SX Phe these are obtained directly from the data (Table 2).

The variable star finding scheme explained in Section 3.1, apart from detecting all the variables from Salinas et al. (2007) within the SAMI FOV, revealed the presence of one previously unknown variable (V31 in Figs. 2 and 3). We find a period of 0.1 days, although this is likely a lower limit, given its proximity to the complete time span of observations. The shape of its light curve, together with its position in the CMD of NGC 1261, slightly above and redder than the upper main sequence (red symbol in the NGC 1261 panel in Fig. 2), suggests its classification as an eclipsing binary, since it is too red to be either a background delta Scuti or an RRc. As an eclisping binary, its period is probably closer to ~ 0.25 days. This variable is about $80''$ from the cluster center, so it was probably missed before due to its faintness, and not because of crowding. Even though this short distance to the center suggests cluster membership its nature as a foreground object cannot be

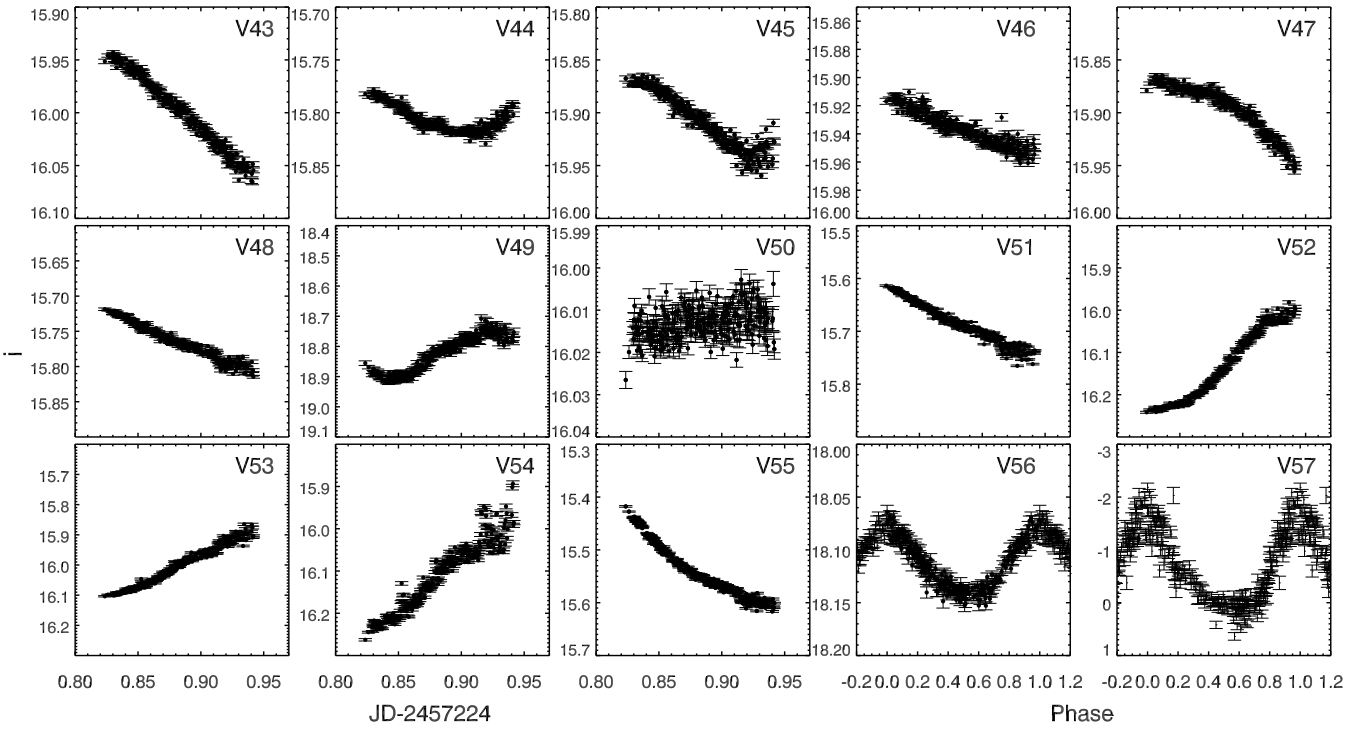

Figure 4. New variables in M 2. Variables V43 to V55 are shown in Julian dates due to our inability to find reliable periods based on the short time span of the observations. V56 is shown phased to the period indicated in Table 3, while V57 is shown phased, but its intensity is given only in relative fluxes (in units of ten thousand ADUs).

ruled out.

Finally, we point out that none of the four BSs where variability was suspected by Simunovic et al. (2014) show signs of variability in our data. The authors of that study suggested the possibility of variability based on the fact that these four BSs had fainter F336W magnitudes than expected, consistent with a potential variability in the F336W magnitude. We note that our SAM photometry of these BSs is consistent to the optical colours and magnitudes given by Simunovic et al. (2014) therefore supporting their characterization in the CMD, in particular for the proposed young collisional products as found by stellar collision model fitting in the CMD. This rather suggests a photometry error in their measured F336W magnitudes, or instead a still unexplained cause for their fainter F336W magnitudes.

4.2. *M 2*

According to the Clement et al. (2001) catalogue of variable stars in Galactic globular clusters (2014 update), M 2 hosts 42 variable stars. Of these, 13 were discovered by the image-subtraction study of Lázaro et al. (2006), who could not transform their relative flux light curves into magnitudes due to an anomalous psf.

We detected all the previously known variables that fall within the SAMI FOV and further discovered 11 new RR Lyrae stars, 1 RRL/W UMa candidate (see below) and 2 SX Phe stars, the latter being the first SX Phe detected in this cluster. Table 3 gives positions, as well as mean magnitudes, amplitudes and classifications. For the RRL, the poor phase coverage prevents us from finding periods and we only give a lower limit. Mean magnitudes and amplitudes are highly uncertain and were derived only using the observed data and not the templates; this implies a large scatter in the colors (see corresponding CMD in Fig. 2), although their position in the CMD makes the classification as RRL unequivocal. The tentaive classification into RRab or RRc is done based on the partial shape of their light curves, hence is also necessarily uncertain. For the SX Phe, these quantities are measured directly from the data.

Fig. 4 shows the light curves of the newly discovered variables. V57, one of the discovered SX Phe, is the only new variable among the four clusters for which we cannot convert the relative flux light curve into magnitudes due to blending. For V49 we measure both the minimum and maximum light phases, showing also the characteristic "hump" before maximum light (Smith 1995; Catelan & Smith 2015). These features would make it most likely a short-period RRc, but its low brightness puts it close to main sequence of the cluster, instead of the HB. This is probably an indication that this is a background variable and not a cluster member. Alternatively, the roughly sinusoidal shape could indicate a contact binary of the W UMa type, although the hump would remain unexplained.

Table 4 contains the variables discovered by Lázaro et al. (2006), all but one inside the SAMI FOV. For these we give new coordinates, mean magnitudes and amplitudes also derived from the template fitting. The latter two quantities were not given by Lázaro et al. (2006).

4.3. *M 10*

The Clement et al. (2001) catalogue lists 4 variables in M 10. Three of them are long-period variables and the fourth, suspected to be an RR Lyrae, lies outside the FOV of this study, although due to its low metallicity

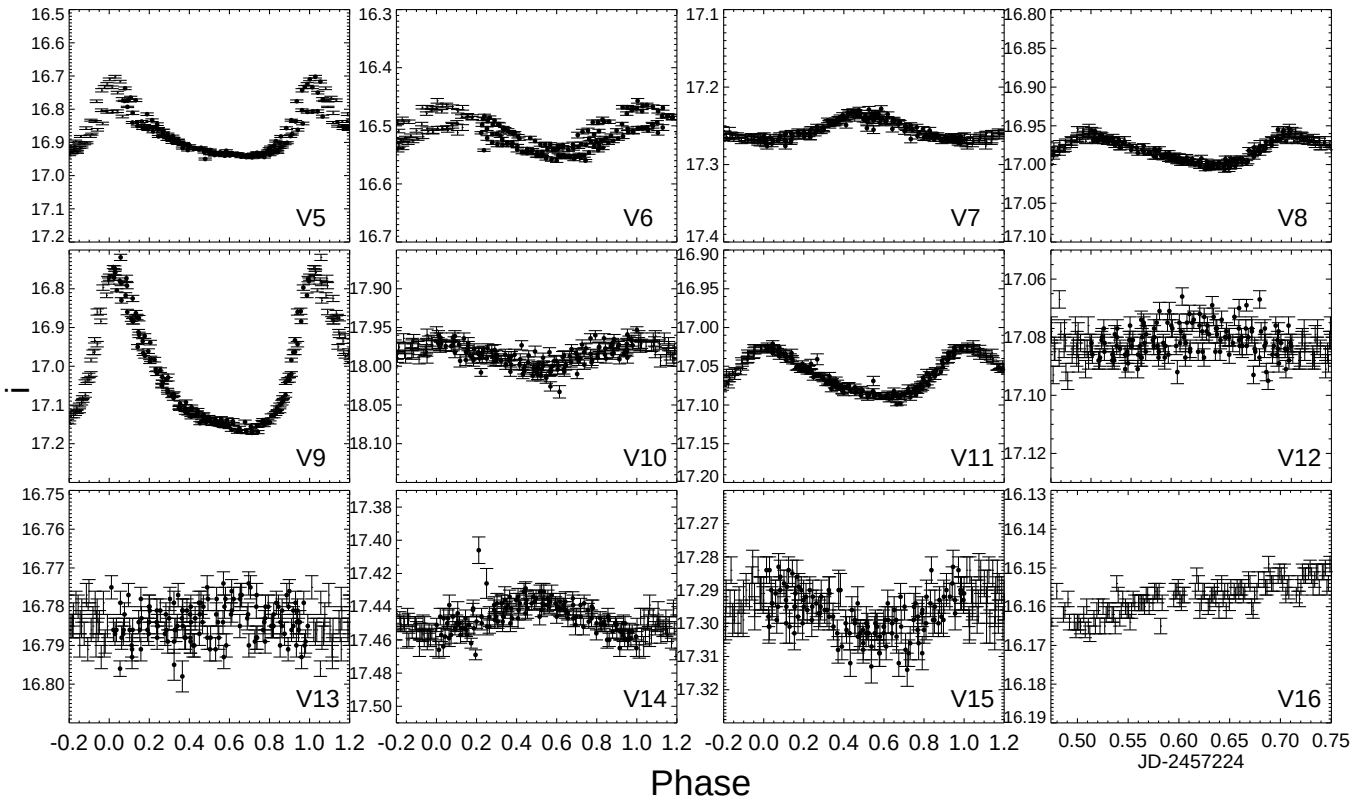

Figure 5. New variables in M 10. V5–V15 are shown phased using the periods given in Table 5, while the light curve of the long period variable V16 is shown in Julian dates only.

and extended blue horizontal branch, few if any RRL are expected. There is no modern CCD-based variability study of this cluster.

Using our data, we found 12 new variables in the M 10 field: 11 SX Phe and a long-period red giant. Positions, periods and amplitudes for all of them are shown in Table 5, while phased light curves for the SX Phe are shown in Fig. 5. Since this cluster has the largest amount of new discoveries with completely sampled light curves, we proceed to a more detailed description of their characteristics.

V5 and V6 present noticeable amplitude changes which hint at pulsation in more than one mode. V5 changes its amplitude by more than 0.1 mag while for V6, the change is close to 0.05 mag. In both cases the time span of observations covers only about 4 pulsation cycles, making it impossible to find frequencies other than the dominant one. McNamara (1995) suggested a broad separation between fundamental and first-overtone pulsators based on the amplitude and shape of the light curve; SX Phe pulsating in the fundamental mode would have amplitudes $\Delta V \geq 0.25$ mag and asymmetrical light curves, while first-overtone pulsators would have more sinusoidal light curves with amplitudes $\Delta V \leq 0.20$. Using the ratio between the amplitudes in V and I, $A_V/A_I = 1.7$ as a guide (Rodríguez et al. 2007; Cohen & Sarajedini 2012), we can classify V5 as a fundamental-mode pulsator and V6 as a first-overtone pulsator.

V7 and V8 show no significant amplitude changes, but while both have very similar amplitudes, $A_i \sim 0.065$, V7 shows a sinusoidal shape, while the light curve of V8 shows the sawtooth-like shape associated with higher-amplitude fundamental pulsators.

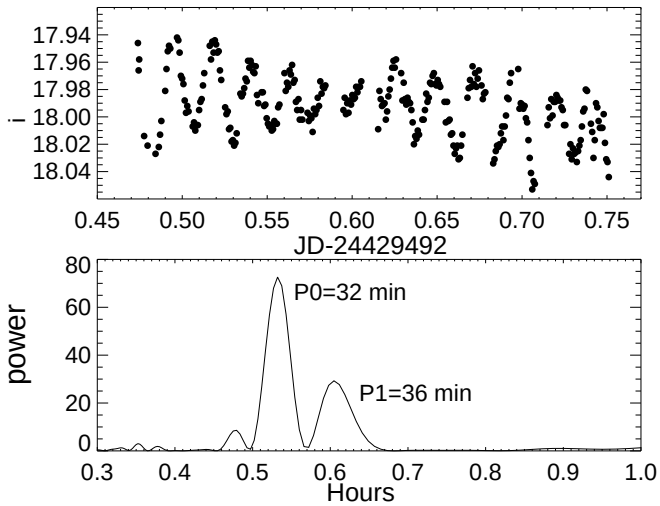

Figure 6. Upper panel: light curve of V10 in M10. Lower panel: Power spectrum of this variable obtained with the Lomb-Scargle algorithm revealing the presence of two close periods in the light curve.

V9 has the largest amplitude of the sample, $A_i = 0.414$, which implies $A_V \sim 0.7$. Its amplitude experiences a change of about 0.1 mag in 5 pulsation cycles, but the Lomb-Scargle exploration does not reveal the presence of another period. From the catalogue of SX Phe in globular clusters by Cohen & Sarajedini (2012) only a handful of SX Phe have larger amplitudes. Large amplitudes are more common among the high-metallicity counterparts of SX Phes, the δ Scuti stars (e.g. Vivas & Mateo 2013), particularly in the subclass of high-amplitude δ Scutis

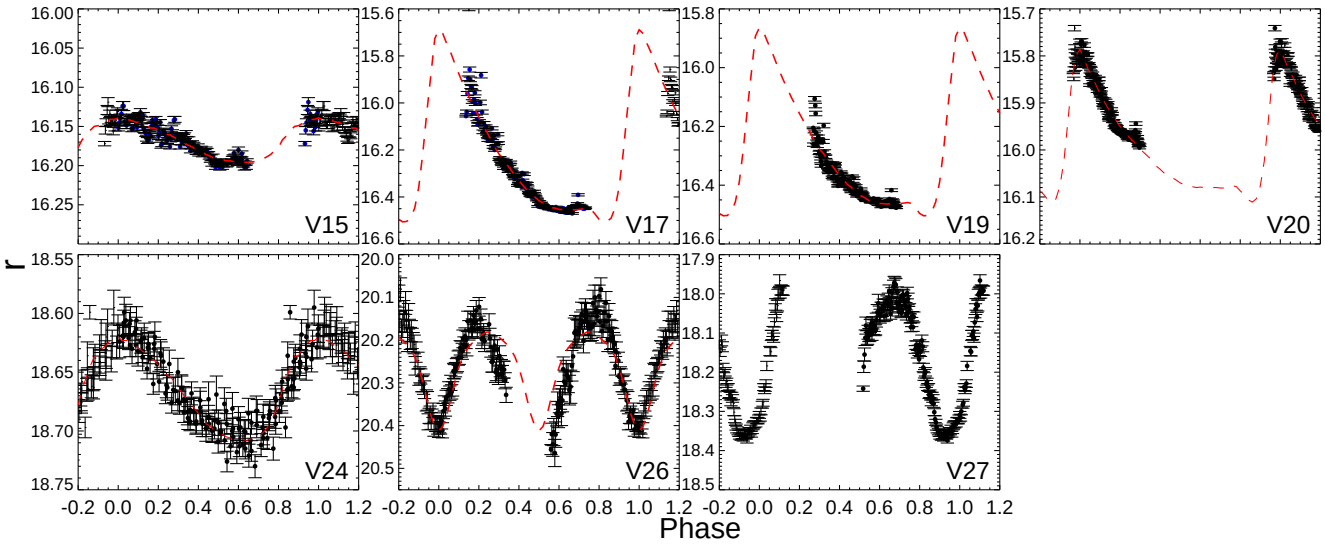

Figure 7. Variables in M 80 that had incomplete information in Kopacki (2013). Dashed lines indicate the best-fit template. This is not shown for V27 where no fit was found satisfactory.

(Catelan & Smith 2015, and references therein). Its very blue color (see Fig. 2), consistent with a star belonging to the extended HB instead of the blue straggler region, is likely an effect of blending in the g band images which have significantly poorer quality compared to the i images. In the *HST* photometry it appears brighter than the BSs of similar color, which could signal it as a foreground object, although its distance of $\sim 25''$ from the cluster center would rather give an indication of cluster membership.

V10 presents some interesting features which make its final classification also uncertain. First, it has a very short main period of 0.022 days. Only two known SX Phe in ω Cen have slightly shorter periods (Kaluzny et al. 2004). Moreover, the Lomb-Scargle analysis reveals the presence of another period of 0.025 days (see Fig. 6). It is fainter than the rest of the SX Phe in M 10 following the expectation from the period-luminosity relation in SX Phe (e.g. McNamara 1995), but it is also bluer than the rest except V9. Like in the case of V9, the bluer color could be explained by partial blending in the g band. The presence of two periods would be associated with two pulsation modes. An alternative explanation could be a HW Vir-type variable, that is, a subdwarf B (sdB) star with a faint eclipsing companion (Menzies & Marang 1986), but the lack of strong flux in the F275W band from the *HST* photometry disfavors the presence of a very hot star.

V11 has no remarkable features other than its sawtooth-like shape, which probably makes it a pulsator in the fundamental mode.

V12 to V15 are unremarkable SX Phe stars with mostly sinusoidal light curves and low amplitudes (~ 0.02 mag) that appear very noisy in the SAM data. They appear well within the BS region in the SAM CMD.

Finally, V16 is located in the lower part of the RGB (see Fig. 2), has a monotonic increase in luminosity with an amplitude $A_i = 0.02$ during the time of observations. We classify it as a long-period variable, a common occurrence among RGB stars, , though its exact nature cannot be established based solely on the present data.

4.4. *M 80*

The Clement et al. (2001) catalogue lists 33 variables in M 80. It was also the host of the only known classical nova in a Galactic GC with convincing evidence, an event which took place in 1860 (Luther 1860), which became known accordingly as Nova 1860 AD or T Scorpii.

Variable star searches in the cluster after the latest Clement catalogue update of 2010 were conducted by Kopacki (2013) and Figuera Jaimes et al. (2016). While Kopacki (2013) found 9 new RRL, 4 SX Phe, two eclipsing binaries and two other periodic variables of unknown type, the work of Figuera Jaimes et al. (2016) found only six new long-period variables.

Our search recovered most of the short-period variables of the previous studies within the SAMI FOV with the exception of V33, an SX Phe discovered by Thomson et al. (2010) very close to the cluster center which was neither recovered by Kopacki (2013), but we did not find any previously unknown variable.

Even though the short time span of our observations does not help in clearing the nature of the variables classified as "unknown" by Kopacki (2013) given their periods larger than two days, we give new colors and magnitudes for the variables V15, V17, V19, V20, V24, V26 and V27, that were not measured by Kopacki (2013) due to difficulties in transforming relative fluxes into magnitudes. The new magnitudes, amplitudes and colors for these variables can be seen in Table 6, while light curves can be seen in Fig. 7. The g magnitude for the variables is simpy taken as the average of the magnitudes in the three g frames, therefore the position of the variables in the CMD (Fig. 2) is very tentative. Finally, our limited observations did not reveal signs of variability either in the vicinity of T Sco or of the other cataclismic variable candidates reported by Shara et al. (2005) and Dieball et al. (2010).

5. M 80: A BLUE STRAGGLER-RICH CLUSTER?

Ferraro et al. (1999) studied the content of blue stragglers in M 80 using the *HST*/WFPC2 filters F225W and F336W. Ultraviolet observations in globular clusters are helpful to study hot stars such as blue stragglers and horizontal branch stars given the lower flux that the other-

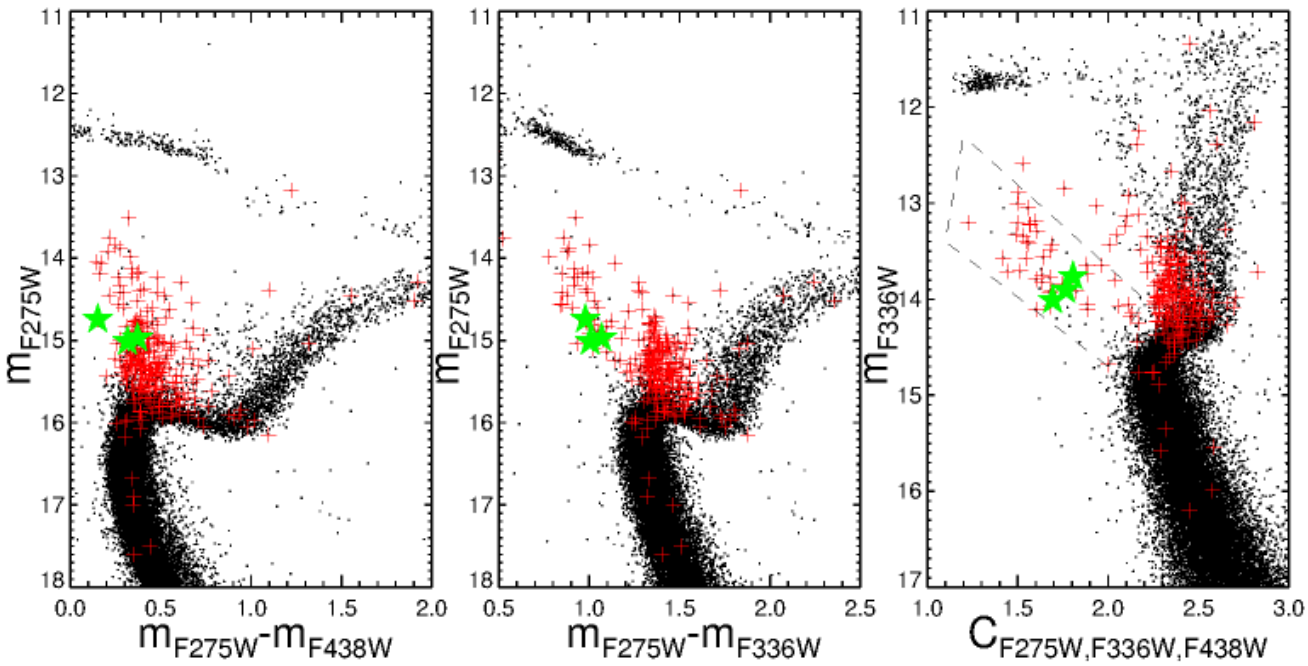

Figure 8. CMD of the blue straggler region in M80 using *HST*/WFC3/UVIS filters F275W, F336W and F438W. BS candidates from Ferraro et al. (1999) are shown in red crosses. Left panel: the F275W–F438W CMD. Central panel: the F275W–F336W CMD. Right panel: the color index $C_{\rm F275W,F336W,F438W}$ gives the best separation for the genuine BSs. The dashed lines define the BS region considered in our study. The three green stars indicate the positions of the SX Phe inside the UVIS FOV.

wise dominant RGB population has in these bandpasses. Based on a color and magnitude selection they found a very high number of 305 BSs within the WFPC2 FOV, that would make it the GC with the highest number of BSs known in the Galaxy.

Ferraro et al. (1999) argued that stellar density, even though very high in the center of this cluster, could not explain by itself this overpopulation of BSs, but instead that the process leading to core collapse enhances the formation of binaries (e.g. Meylan & Heggie 1997) that goes in hand with an increase in the number of BSs.

This view was challenged by Dieball et al. (2010) who, using *HST*/ACS FUV and NUV filters found only 75 BSs, the same number as in M 15, making M 80 unremarkable regarding its BSs content.

Using newly available *HST*/UVIS data of M80 obtained in the filters F275W, F336W and F436W, we reassess the BS content of M80. Using the UVIS photometry from Section 2.2 we constructed color-magnitude diagrams, cross-matching the positions of the BS candidates from Ferraro et al. (1999) to our photometry using CataXcorr/CataComb. BS candidates from Ferraro et al. (1999) are shown in Fig. 8 as red crosses.

The different panels in Fig. 8 show how the blue straggler region is populated differently depending on the bandpasses used. In the F275W–F436W color, most of the candidates from Ferraro et al. (1999) fall inside the BS region (left panel), but using the bluer color F275W–F336W already reveals a separation between blue stragglers and a population of fainter "yellow stragglers" (Hesser et al. 1984), with colors slightly redder than the MSTO (middle panel). Finally, using the pseudo-color $C_{\rm F275W,F336W,F438W} = (m_{\rm F275W} - m_{\rm F336W}) - (m_{\rm F336W} - m_{\rm F438W})$, which has been shown to be very effective to separate multiple stellar populations (Milone et al. 2013; Piotto et al. 2015), the separation between the real blue stragglers and this yellow population is clearly established.

"Yellow stragglers" can be considered as the evolution of BSs (e.g. Landsman et al. 1997), but in this case the very narrow color range they occupy, considered in tandem with the very high central density, points rather to blends due to crowding, despite the resolving power of *HST*.

Using the $C_{\rm F275W,F336W,F438W}$ color index we make a new determination of the number of BSs in M80. We consider as BSs the stars within the bounding box shown in Fig. 8 (right panel) counting up to 79 stars in good agreement with Dieball et al. (2010). The significance of this number can be assessed by comparing to a control population within the cluster. In particular, following Ferraro et al. (1999), we define the specific frequency of BSs as the ratio to horizontal branch stars, $F_{\rm HB}^{\rm BSS} = N_{\rm BSS}/N_{\rm HB} = 0.22$. If we consider the specfic frequencies derived for 56 GCs by Piotto et al. (2004), clusters with luminosities similar to M80 have a range of $0.15 \lesssim F_{\rm HB}^{\rm BSS} \lesssim 0.4$, indicating that the specific frequency in M 80 is normal. Furthermore, our variability study (Section 4.4) and the previous variability studies (Kopacki 2013; Figuera Jaimes et al. 2016) do not reveal the presence of a large amount of binaries (including eclipsing binaries) that should also be enhanced during a state prior to core collapse (e.g. Meylan & Heggie 1997) and that should be readily detectable. We therefore conclude that M 80 does not host an unusually large number of BSs and may not be close to core collapse, in contrast to the early claim of Ferraro et al. (1999).

6. SUMMARY AND CONCLUSIONS

In this paper we presented time-series photometry of four globular clusters: M 2, M 10, M 80 and NGC 1261. These images were obtained using SAM, the adaptive

optics module at the SOAR Telescope. The correction of the ground-layer turbulence done by SAM provides sharper images, which allow absolute photometry closer to the centers of globular clusters than non-AO ground-based observations, and in this way a larger number of light curves obtained through image subtraction can be calibrated to magnitudes.

We studied the four clusters using the image subtraction technique (Alard & Lupton 1998), finding in total 28 new variables. In M 2, we discovered 12 new RRL stars and 3 SX Phe stars. In M 10, we found 11 SX Phe stars and one long-period variable, while in NGC 1261 we found an eclipsing W UMa-type variable. The light curves of all but one of these new variables were transformed into magnitudes.

We also reviewed the claim that M 80 is the GC with the highest number of BSs in our Galaxy. Based on *HST*/UVIS data we found $\sim$ 80 BSs, significantly less than the 305 announced by Ferraro et al. (1999), suggesting that the cluster may have a lower specific fraction of BSs than previously suspected.

In summary, we have shown that ground-layer AO-assisted imaging has the potential to pierce deeper into crowded environments than normal ground-based observations, being very helpful for the detection and calibration of variable stars. Even though the image quality delivered by SAM cannot rival the power of *HST*, the possibility to use it for longer periods of time makes it a very good match to variability and monitoring programs in crowded environments. Furthermore, the performance of image subtraction against high surface brightness backgrounds (e.g. within distant galaxies) has been shown to be greatly improved when sharper image quality is used (e.g. Rau et al. 2008; Kerins et al. 2010).

We thank the anonymous referee for a fast report that helped improve the presentation of our results. We thank Andrei Tokovinin and César Briceño for their assistance during the SOAR/SAM runs. JS acknowledges partial support from NSF grant AST-1308124 and the Packard Foundation. Support for M.C. and R.C.R. is provided by the Ministry for the Economy, Development, and Tourism's Millennium Science Initiative through grant IC 120009, awarded to the Millennium Institute of Astrophysics (MAS). M.C. acknowledges additional support by Proyecto Basal PFB-06/2007 and by FONDECYT grant #1141141. Supported by the Gemini Observatory, which is operated by the Association of Universities for Research in Astronomy, Inc., on behalf of the international Gemini partnership of Argentina, Brazil, Canada, Chile, and the United States of America. Based on observations made with the NASA/ESA Hubble Space Telescope, obtained from the data archive at the Space Telescope Science Institute. STScI is operated by the Association of Universities for Research in Astronomy, Inc. under NASA contract NAS 5-26555.

Facility: SOAR

REFERENCES

Alard, C. 2000, A&AS, 144, 363
Alard, C., & Lupton, R. H. 1998, ApJ, 503, 325
Anderson, J., & King, I. R. 2006, PSFs, Photometry, and Astronomy for the ACS/WFC, Tech. rep.
Baldacci, L., Rizzi, L., Clementini, G., & Held, E. V. 2005, A&A, 431, 1189
Bellini, A., Anderson, J., & Bedin, L. R. 2011, PASP, 123, 622
Catelan, M., & Smith, H. A. 2015, Pulsating Stars
Catelan, M., Smith, H. A., Pritzl, B. J., et al. 2006, Mem. Soc. Astron. Italiana, 77, 202
Catelan, M., Minniti, D., Lucas, P. W., et al. 2013, in 40 Years of Variable Stars: A Celebration of Contributions by Horace A. Smith (ed. K. Kinemuchi et al.), 139, arXiv:1310.1996
Clement, C. M., Muzzin, A., Dufton, Q., et al. 2001, AJ, 122, 2587
Cohen, R. E., & Sarajedini, A. 2012, MNRAS, 419, 342
Contreras, R., Catelan, M., Smith, H. A., Pritzl, B. J., & Borissova, J. 2005, ApJ, 623, L117
Corwin, T. M., Catelan, M., Borissova, J., & Smith, H. A. 2004, A&A, 421, 667
Corwin, T. M., Sumerel, A. N., Pritzl, B. J., et al. 2006, AJ, 132, 1014
Dieball, A., Long, K. S., Knigge, C., Thomson, G. S., & Zurek, D. R. 2010, ApJ, 710, 332
Eggen, O. J. 1952, PASP, 64, 305
Ferraro, F. R., Paltrinieri, B., Rood, R. T., & Dorman, B. 1999, ApJ, 522, 983
Figuera Jaimes, R., Bramich, D. M., Skottfelt, J., et al. 2016, A&A, 588, A128
Fraga, L., Kunder, A., & Tokovinin, A. 2013, AJ, 145, 165
Hesser, J. E., McClure, R. D., Hawarden, T. G., et al. 1984, PASP, 96, 406
Kaluzny, J., Olech, A., Thompson, I. B., et al. 2004, A&A, 424, 1101
Kerins, E., Darnley, M. J., Duke, J. P., et al. 2010, MNRAS, 409, 247
Kopacki, G. 2013, Acta Astronomica, 63, 91
Kunder, A., Chaboyer, B., & Layden, A. 2010, AJ, 139, 415
Kunder, A., Stetson, P. B., Catelan, M., Walker, A. R., & Amigo, P. 2013, AJ, 145, 33
Landolt, A. U. 1992, AJ, 104, 340
Landsman, W., Aparicio, J., Bergeron, P., Di Stefano, R., & Stecher, T. P. 1997, ApJ, 481, L93
Layden, A. C. 1998, AJ, 115, 193
Lázaro, C., Arellano Ferro, A., Arévalo, M. J., et al. 2006, MNRAS, 372, 69
Luther. 1860, Astronomische Nachrichten, 53, 293
McNamara, D. H. 1995, AJ, 109, 1751
Menzies, J. W., & Marang, F. 1986, in IAU Symposium, Vol. 118, Instrumentation and Research Programmes for Small Telescopes, ed. J. B. Hearnshaw & P. L. Cottrell, 305
Meylan, G., & Heggie, D. C. 1997, A&A Rev., 8, 1
Milone, A. P., Marino, A. F., Piotto, G., et al. 2013, ApJ, 767, 120
Piotto, G., De Angeli, F., King, I. R., et al. 2004, ApJ, 604, L109
Piotto, G., Milone, A. P., Bedin, L. R., et al. 2015, AJ, 149, 91
Rau, A., Ofek, E. O., Kulkarni, S. R., et al. 2008, ApJ, 682, 1205
Rodríguez, E., Fauvaud, S., Farrell, J. A., et al. 2007, A&A, 471, 255
Salinas, R., Catelan, M., Smith, H. A., & Pritzl, B. J. 2007, Information Bulletin on Variable Stars, 5744, 1
Salinas, R., Catelan, M., Smith, H. A., Pritzl, B. J., & Borissova, J. 2005, Information Bulletin on Variable Stars, 5640, 1
Salinas, R., Jílková, L., Carraro, G., Catelan, M., & Amigo, P. 2012, MNRAS, 421, 960
Scargle, J. D. 1982, ApJ, 263, 835
Shara, M. M., Hinkley, S., & Zurek, D. R. 2005, ApJ, 634, 1272
Simunovic, M., Puzia, T. H., & Sills, A. 2014, ApJ, 795, L10
Smith, H. A. 1995, RR Lyrae Stars (Cambridge)
Stellingwerf, R. F. 1978, ApJ, 224, 953
Stetson, P. B. 1987, PASP, 99, 191
Stetson, P. B. 1993, in IAU Colloq. 136: Stellar Photometry - Current Techniques and Future Developments, ed. C. J. Butler & I. Elliott, 291
—. 1994, PASP, 106, 250
Taylor, M. B. 2006, in Astronomical Society of the Pacific Conference Series, Vol. 351, Astronomical Data Analysis Software and Systems XV, ed. C. Gabriel, C. Arviset, D. Ponz, & S. Enrique, 666
Thomson, G. S., Dieball, A., Knigge, C., Long, K. S., & Zurek, D. R. 2010, MNRAS, 406, 1084
Tokovinin, A., Cantarutti, R., Tighe, R., et al. 2010, PASP, 122, 1483

Tokovinin, A., Tighe, R., Schurter, P., et al. 2012, in Society of Photo-Optical Instrumentation Engineers (SPIE) Conference Series, Vol. 8447
Tomaney, A. B., & Crotts, A. P. S. 1996, AJ, 112, 2872
Vivas, A. K., & Mateo, M. 2013, AJ, 146, 141
Walraven, T. 1953, Bull. Astron. Inst. Netherlands, 12, 57
Wehlau, A., & Demers, S. 1977, A&A, 57, 251
Wehlau, A., Flemming, T., Demers, S., & Bartolini, C. 1977, Information Bulletin on Variable Stars, 1361, 1
Zacharias, N., Finch, C., Girard, T., et al. 2010, AJ, 139, 2184

Table 2
Variables in NGC 1261

ID	RA (J2000)	Dec (J2000)	$\langle r \rangle$	A_r	P(d)	Type
V22	03 12 16.49	–55 13 38.10	17.00:	0.21:	0.302	RRc
V24	03 12 14.43	–55 13 34.77	16.97:	0.83:	0.626	RRab
V26	03 12 17.05	–55 12 43.92	18.66	0.12	0.0799	SXPhe
V27	03 12 14.65	–55 13 06.50	16.73:	0.11:	0.341	RRc
V28	03 12 13.53	–55 13 00.80	17.00:	0.15:	0.287	RRc
V29	03 12 13.05	–55 13 20.45	16.98:	0.15:	0.593	RRab
V30	03 12 16.58	–55 12 53.96	18.42	0.07	0.0591	SXPhe
V31	03 12 18.70	–55 14 16.00	20.59	0.16	> 0.1	W UMa?

Note. — The table contains all the variables discovered by Salinas et al. (2007) in the SAMI FOV that were not saturated, plus the newly found V31. For the known variables, periods and classification are taken from Salinas et al. (2007). Colons indicate uncertain values.

Table 3
New variables in M 2

ID	RA (J2000)	Dec (J2000)	$\langle i \rangle$	A_i	P(d)	Type
V43	21 33 26.44	–00 49 29.3	16.00:	> 0.12	> 0.12	RRab?
V44	21 33 26.69	–00 49 21.8	15.81:	> 0.05	> 0.12	RRc?
V45	21 33 26.13	–00 49 22.2	15.91:	> 0.09	> 0.12	RRab?
V46	21 33 27.45	–00 49 15.5	15.94:	> 0.05	> 0.12	RRab?
V47	21 33 27.40	–00 49 05.4	15.91:	> 0.09	> 0.12	RRc?
V48	21 33 27.51	–00 49 07.5	15.76:	> 0.10	> 0.12	RRab?
V49	21 33 30.45	–00 50 29.6	18.82:	~ 0.20	> 0.12	RRc?/W UMa?
V50	21 33 26.63	–00 49 11.2	16.01:	> 0.03	> 0.12	RRc?
V51	21 33 24.94	–00 48 43.3	15.68:	> 0.14	> 0.12	RRab?
V52	21 33 25.12	–00 49 24.4	16.12:	~ 0.26	> 0.12	RRc?
V53	21 33 28.24	–00 49 35.4	16.00:	> 0.24	> 0.12	RRc?
V54	21 33 27.55	–00 49 29.1	16.11:	> 0.36	> 0.12	RRab?
V55	21 33 26.37	–00 49 18.1	15.54:	> 0.20	> 0.12	RRab?
V56	21 33 31.62	–00 50 13.0	18.11	0.10	0.0468	SX Phe
V57	21 33 27.54	–00 49 21.4	–	–	0.0686	SX Phe

Note. — The table contains all the new variables discovered in M 2. Colons indicate uncertain values.

Table 4
Variables in M 2 from Lázaro et al. (2006)

ID	RA (J2000)	Dec (J2000)	$\langle i \rangle$	A_i	P(d)	Type
V36	21 33 30.71	-00 49 13.5	16.21:	0.08:	0.27078	RRc
V37	21 33 26.04	-00 49 18.1	15.79:	0.19:	0.56668	RRab
V38	21 33 31.20	-00 49 23.8	15.84:	0.23:	0.80735	RRab
V39	21 33 27.38	-00 50 07.2	16.08:	0.13:	0.60781	RRab
V40	21 33 25.66	-00 49 16.3	16.11:	0.18:	0.75173	RRab
V41	21 33 28.02	-00 49 24.3	15.68:	0.32:	0.60532	RRab
V42	21 33 28.42	-00 49 54.6	16.09:	0.27:	0.32801	RRc

Note. — Periods and classification are from Lázaro et al. (2006), while positions, mean magnitudes and amplitudes come from this work. Colons indicate uncertain values.

Table 5
New variables in M 10

ID	RA (J2000)	Dec (J2000)	$\langle i \rangle$	A_i	P(d)	Type
V5	16 57 08.59	–04 06 16.3	16.875	0.267	0.058	SX Phe
V6	16 57 10.71	–04 05 33.3	16.499	0.115	0.060	SX Phe
V7	16 57 10.35	–04 07 03.0	17.251	0.051	0.048	SX Phe
V8	16 57 08.29	–04 05 10.0	16.978	0.055	0.051	SX Phe
V9	16 57 10.65	–04 05 50.8	17.040	0.414	0.051	SX Phe/ δ Sct?
V10	16 57 08.43	–04 06 54.7	17.977	0.086	0.022	SX Phe/HW Vir?
V11	16 57 10.81	–04 05 55.9	17.064	0.078	0.048	SX Phe
V12	16 57 04.04	–04 06 06.9	17.091	0.020	0.023	SX Phe
V13	16 57 08.80	–04 06 24.5	16.775	0.016	0.036	SX Phe
V14	16 57 09.20	–04 06 05.3	17.449	0.066	0.038	SX Phe
V15	16 57 13.28	–04 05 48.7	17.297	0.031	0.035	SX Phe
V16	16 57 06.21	–04 06 42.2	16.16:	0.02:	> 0.3	LPV?

Note. — The table contains all the new variables discovered in M 10. Colons indicate uncertain values.

Table 6
Variables in M 80

ID	RA (J200)	Dec (J2000)	$\langle r \rangle$	A_r	P(d)	Type
V15	16 17 04.04	–22 58 40.2	16.17:	0.08:	0.3479	RRc
V17	16 17 04.61	–22 58 40.0	16.20:	0.82:	0.4154	RRc
V19	16 17 02.11	–22 58 29.5	16.28:	0.64:	0.5956	RRab
V20	16 17 03.26	–22 58 37.5	16.00:	0.32:	0.7448	RRab
V24	16 17 02.99	–22 59 21.1	18.67	0.13	0.04941	SX Phe
V26	16 17 04.49	–22 59 17.9	20.27:	0.38:	0.3190	W UMa
V27	16 17 04.02	–22 58 26.5	18.13:	0.41:	0.4117	W UMa

Note. — The tables contains variables from Kopacki (2013) that had incomplete information. Position, classification and periods come from Kopacki (2013), while mean magnitudes and amplitudes are from the present study. Colons indicate uncertain values.